Channel variability measurements in an underwater acoustic network

Mandar Chitre*† and Konstantinos Pelekanakis†

* Department of Electrical & Computer Engineering, National University of Singapore.
† ARL, Tropical Marine Science Institute, National University of Singapore.

***Abstract*—The MISSION 2013 experiment was held in Singapore in November 2013. During the experiment, channel measurements were made across several network links over many days. We present preliminary channel variability analysis at two timescales for five network links over a three day period. We find that the variability in signal strength across different multipath arrivals is weakly correlated. We also observe that weaker arrivals usually exhibit more variability at a short timescale. At longer timescales, variability increases with surface and bottom interactions.**

I. Introduction

UNDERWATER acoustic channels exhibit a high degree of temporal and spatial variability, especially in shallow coastal areas. Recent years have seen a growing interest in understanding, modeling and simulating this variability [1]–[7]. Analysis of data from several experiments has led to statistical models that efficiently simulate time-varying channel impulse responses [4]. These models accurately predict the statistics of individual multipath arrivals, they do not model the correlation between multiple arrivals or across multiple network links. Such correlations can arise from common environmental factors that directly affect multiple paths or links.

In order to understand time-variability of the underwater acoustic channel across multiple links, and its impact on network performance, the MISSION 2013 experiment was conducted in Singapore in November 2013. The experiment involved multiple underwater networks with static and mobile nodes operating concurrently. Several environmental sensors were also deployed in the area, so that a rich communication and environmental dataset was obtained for statistical analysis. In this paper, we present preliminary analysis of channel variability measurements made as part of the experiment. We start by estimating variability in channel impulse response over at timescales of tens of milliseconds. We not only study the variability of individual arrivals in the multipath, but also explore correlations between arrivals. We then extend the variability analysis to long timescales by studying long term distribution of the parameters describing the short timescale variability.

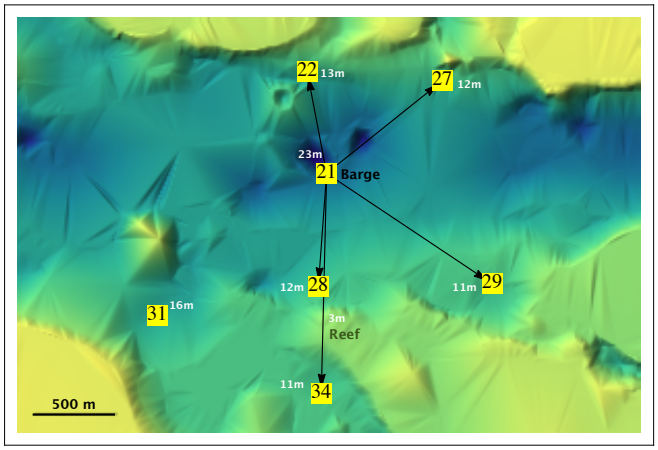

Fig. 1. UNET network node locations during the MISSION 2013 experiment (deployment #2). Yellow squares are network nodes. Water depths are marked in white at selected areas.

The paper is organized as follows. In section II, we describe the experimental setup. In section III, we explain how we estimate the channel and process the experimental data. We then present the short timescale channel variability results in section IV-A. Next we analyze the dependency between multipath arrivals in section IV-B. We then present long timescale channel variability analysis is section IV-C. Finally we summarize our findings in section V.

II. Experimental Setup

The MISSION 2013 experiment was conducted at Selat Pauh in Singapore waters from 15th to 29th November 2013. Several underwater communication techniques, network protocols, and localization algorithms were tested during the experiment. In this paper, we focus our attention on channel measurements made over a 3-day period from 26th to 28th November.

The UNET network deployed during the experiment consisted of a UNET-2 modem [8] (node 21) mounted 6 meters below a barge, and six UNET-PANDA nodes [5] (nodes 22, 27, 28, 29, 31 and 34) deployed at various locations within a 2×2 km area around the barge. In this paper, we restrict our study to 485 channel measurements on five of the network links originating at node 21 as shown in Fig. 1. The water depth in the area ranged from 23 m near the barge to about 3 m at the reef. Most of the UNET-PANDA nodes were in about 10-15 m water depth, deployed about 3 m above the seabed.

III. Channel Estimation

For channel measurement, a 650 ms probe signal was transmitted from the source node and received on all other network nodes. The probe signal consisted of a 17 kbps BPSK-modulated m-sequence. Prior to transmission, the signal was modulated onto a 25.5 kHz carrier. This resulted in a signal that occupied the band 17–34 kHz. At the receiving nodes, the received signal was shifted to baseband, low-pass filtered and sampled at 1 sample/symbol.

The channel estimation algorithm uses each received signal to produce a time-varying estimate of the channel. The baseband probe signal is used as the reference signal. A filter length of 172 taps is required to capture the entire multipath spread of the channel. The filter taps are computed via the improved proportionate M-estimate affine projection algorithm (IPMAPA). This algorithm combines Hampel's three-part redescending M-estimate of the channel prediction error with natural gradient adaptation. This combination achieves robustness against the impulsive noise due to snapping shrimp in Singapore waters, while exploiting varying degrees of channel sparsity [9]. We only consider the channel estimate once the mean absolute error (MAE) of the estimator reduces to within 10% of its stable value[1], and decimate the estimator output to obtain a channel estimate every 1 ms. An example impulse response estimated from a single probe transmission from node 21 to node 28 is shown in Fig. 2. We can see that the channel is clearly sparse with a number of distinct arrivals. This is true for all five links over the three day period.

For each link, we identify 3 stable arrivals (denoted as A, B and C). These arrivals may vary in terms of amplitude and multipath delay, but are 'stable' in the sense that they can be consistently identified over the entire dataset. Arrival A is always the first arrival, while arrivals B and C are later stable arrivals (not necessarily the second and third arrivals). Fig. 3 shows the selected arrivals on a series of impulse responses over the three day period on one of the links. We denote the complex tap coefficient at time t ms for arrival a estimated using probe transmission i as h_{ita}.

[1]The typical steady-state value of MAE is about 0.5 when normalized by the average amplitude of the received signal.

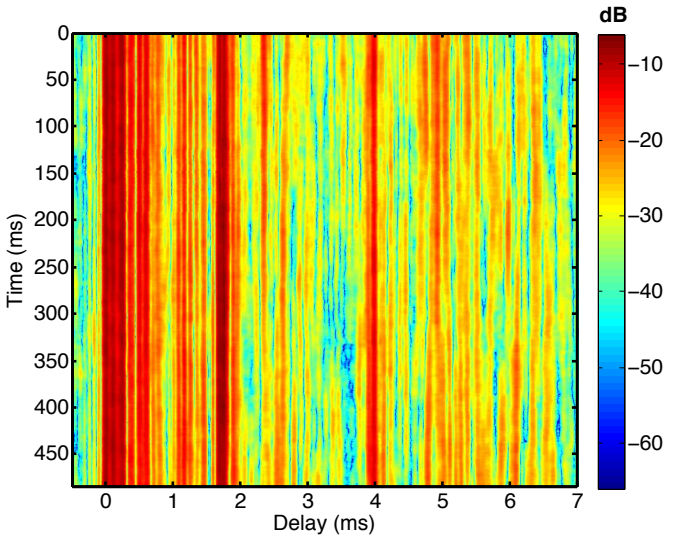

Fig. 2. Short time-scale impulse response variability estimated from a single probe transmission #20 from node 21 to node 28. The x-axis shows the multipath delay and the y-axis shows time.

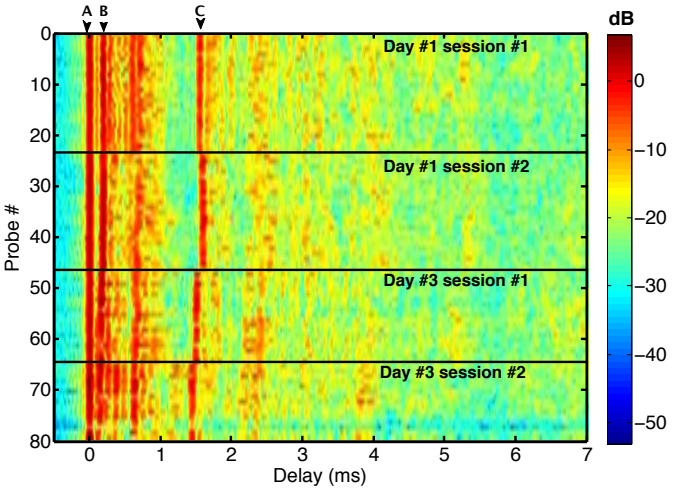

Fig. 3. Long time-scale impulse response variability estimated from a series of probe transmissions from node 21 to node 22. Three arrivals A, B and C used for further analysis are marked by arrows at the top.

IV. Channel Variability

A. Short timescale variability

Each probe provides us a channel estimate every 1 ms for about 500 ms. We call the variability within each probe as the *short timescale variability*. As shown in Fig. 2, the arrival time does not vary significantly over this timescale. However, the tap amplitude $|h_{ita}|$ exhibits

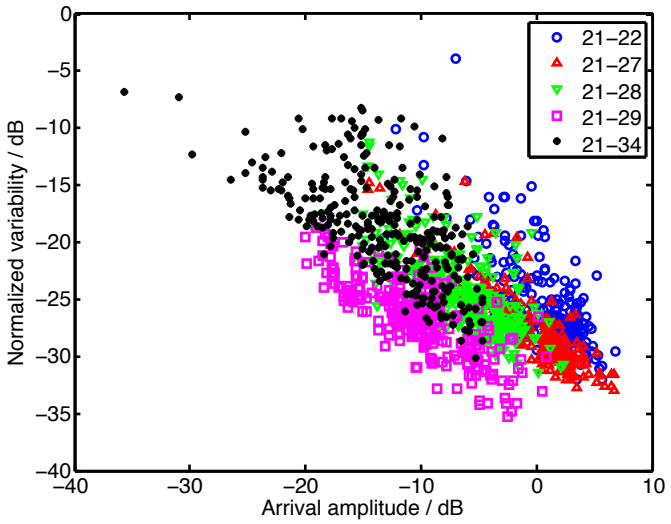

Fig. 4. A plot of normalized variability ν_{ia} against average arrival amplitude μ_{ia} for all arrivals across all links shows a near-linear dependence with weaker arrivals exhibiting more variability.

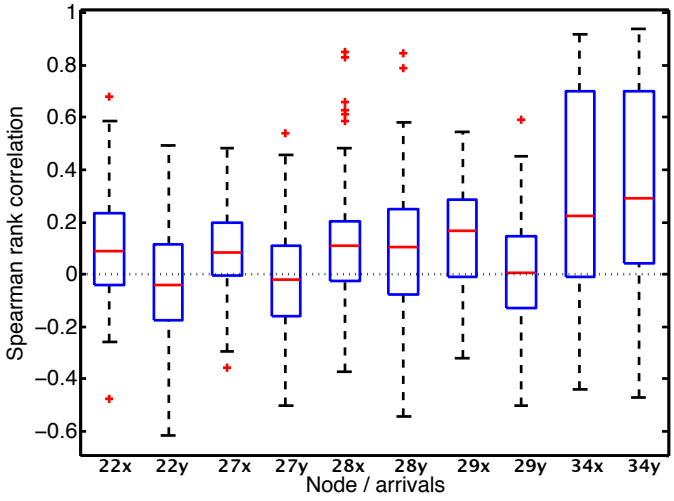

Fig. 5. A boxplot showing the distribution of Spearman rank correlation coefficients $\{\rho_{iab}\forall i\}$ for each link and arrival pair label. The link is from node 21 to the specified node. The arrival pair label 'x' represents the correlation between the arrivals A and B, i.e., $\{\rho_{iAB}\forall i\}$. The label 'y' represents the correlation between arrivals A and C, i.e., $\{\rho_{iAC}\forall i\}$. The boxplot shows the median value as a red horizontal bar in each blue box representing the quartile range (25% to 75% percentile). The full range of data is denoted by the whiskers, and outliers are marked as individual points.

variability. For most of the probe receptions, we find that the short timescale variability is well approximated by a Gaussian distribution. This is consistent with [4], where the authors find that the arrival amplitude variability can be modeled using a Rician distribution – when the mean is large as compared to the variability, the Gaussian and Rician distributions are practically indistinguishable.

For each probe transmission i, we compute the average arrival amplitude μ_{ia} and normalized variability ν_{ia}:

$$\mu_{ia} = \frac{1}{T}\sum_{t=0}^{T-1}|h_{ita}|\,, \tag{1}$$

$$\nu_{ia}^2 = \frac{1}{T}\sum_{t=0}^{T-1}\left(\frac{|h_{ita}|-\mu_{ia}}{\mu_{ia}}\right)^2, \tag{2}$$

where T is the number of impulse response estimates available from a single probe. Normalized variability ν_{ia} is simply the standard deviation of $\{|h_{ita}|\,\forall t\}$ normalized by the mean amplitude μ_{ia}. A plot of ν_{ia} against μ_{ia} is shown in Fig. 4 for all i and a. We observe that weaker arrivals generally exhibit more variability.

B. Interarrival correlation

Most statistical models based on ray theory assume that random fading along each ray path is independent of all other ray paths. This leads to arrival amplitudes that are statistically independent and uncorrelated.

To check if the arrival amplitudes are indeed independent of other arrivals, we compute the Spearman rank correlation coefficient ρ_{iab} between $\{|h_{ita}|\,\forall t\}$ and $\{|h_{itb}|\,\forall t\}$ [10]. The Spearman correlation was chosen over the Pearson correlation since it has the advantage of being non-parametric, and it is more robust to outliers. A boxplot for the distribution of ρ_{iab} for various links and ab-pairs is shown in Fig. 5.

Except for a few isolated cases, we find that the arrivals are not independent. This may be due to propagation conditions in the space close to the transmitter or receiver, since that space is shared by all arrivals. While the correlation is generally weak, it can occasionally be quite strong. This may be due to sporadic events that strongly affect the propagation conditions in that space.

The correlations for link 21-34 are significantly stronger than for other links. This may be due to the fact that the link passes over a reef, where all ray paths between the nodes pass through the same small volume of water.

C. Long timescale variability

Next, we study the distribution of the short timescale parameters μ_{ia} and ν_{ia} over a longer timescale of three days. Fig. 6 shows the statistics of mean arrival amplitude $\{\mu_{ia}\forall i\}$ as a function of the link and arrival a.

For all links except link 21-34, preliminary ray-tracing suggests that arrival A is the direct path, arrival B is the surface reflection, and arrival C includes a bottom interaction. The direct path exhibits the least variability at this timescale. The surface-reflected path is, on an average, as strong as the direct path, and occasionally stronger (perhaps due to focusing from waves). The

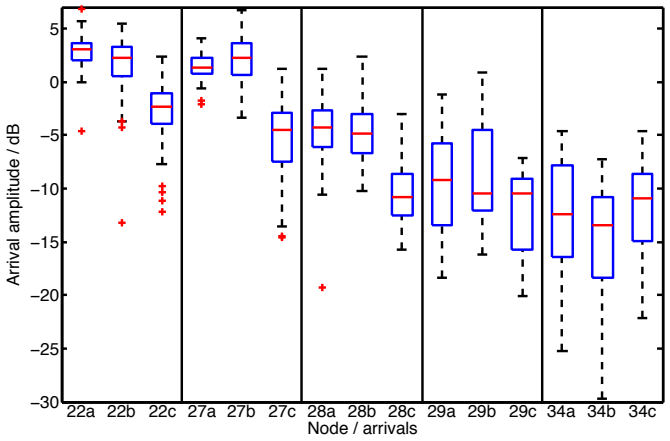

Fig. 6. A boxplot showing the distribution of mean arrival amplitude $\{\mu_{ia}\forall i\}$ for each link and arrival a. Each link is specified by the destination node address. The arrival labels 'a', 'b' and 'c' denote arrivals A, B and C respectively. The boxplot shows the median value as a red horizontal bar in each blue box representing the quartile range (25% to 75% percentile). The full range of data is denoted by the whiskers, and outliers are marked as individual points.

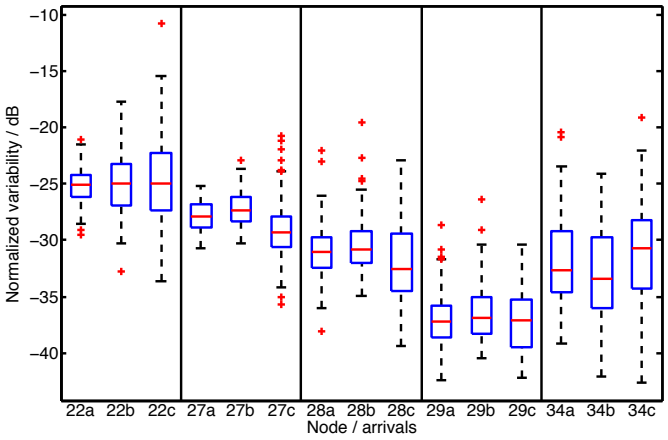

Fig. 7. A boxplot showing the distribution of arrival variability $\{\nu_{ia}\forall i\}$ for each link and arrival a. Each link is specified by the destination node address. The arrival labels 'a', 'b' and 'c' denote arrivals A, B and C respectively. The boxplot shows the median value as a red horizontal bar in each blue box representing the quartile range (25% to 75% percentile). The full range of data is denoted by the whiskers, and outliers are marked as individual points.

bottom-reflected path typically shows an average loss of about 6 dB as compared to the direct path.

For link 21-34, the reef quite likely blocks the line-of-sight. Arrival A therefore is likely to be a surface reflection, and arrivals B and C include some bottom interactions.

Fig. 7 shows the statistics of normalized arrival variability $\{\nu_{ia}\forall i\}$ as a function of the link and arrival a. We find that the variability, on an average, is similar for all arrivals but differs significantly across links. This can be seen by comparing the median normalized variability (red horizontal bar) across arrivals and links in Fig. 7. The long term variation of ν_{ia} is higher for surface-reflected and bottom-reflected arrivals, as compared to the direct arrival.

V. Conclusions

We presented preliminary analysis of 485 channel measurements during the MISSION 2013 experiment. The analysis suggests that the short timescale variability of strong multipath arrivals can be modeled as a Gaussian or Rician random variable. While this finding is in agreement with existing literature [4], we additionally find that variability of different multipath arrivals is not independent. A correlation between various multipath arrivals has to be included in an accurate statistical channel model. We also find that stronger arrivals usually vary less (in relative terms) as compared to weaker arrivals. At longer timescales, we find that the direct arrival is typically the less variable (more stable) although it may not always be the strongest. The surface-reflected arrival can be as strong as the direct arrival, or even stronger, but it exhibits more variability. The average short timescale variability of all arrivals is about the same, but varies significantly across links.

References

[1] M. Badiey, Y. Mu, J. Simmen, and S. Forsythe, "Signal variability in shallow-water sound channels," *Oceanic Engineering, IEEE Journal of*, vol. 25, no. 4, pp. 492–500, Oct 2000.

[2] A. Song, M. Badiey, H. C. Song, W. S. Hodgkiss, M. B. Porter, and KauaiEx-Group, "Impact of ocean variability on coherent underwater acoustic communications during the kauai experiment (kauaiex)," *The Journal of the Acoustical Society of America*, vol. 123, no. 2, pp. 856–865, 2008.

[3] C. T. Tindle, G. B. Deane, and J. C. Preisig, "Reflection of underwater sound from surface waves," *The Journal of the Acoustical Society of America*, vol. 125, no. 1, pp. 66–72, 2009.

[4] P. Qarabaqi and M. Stojanovic, "Statistical characterization and computationally efficient modeling of a class of underwater acoustic communication channels," *Oceanic Engineering, IEEE Journal of*, vol. 38, no. 4, pp. 701–717, 2013.

[5] M. Chitre, I. Topor, R. Bhatnagar, and V. Pallayil, "Variability in link performance of an underwater acoustic network," in *Proceedings of IEEE OCEANS 2013 Bergen*, June 2013.

[6] H. Dol, M. Colin, M. Ainslie, P. van Walree, and J. Janmaat, "Simulation of an underwater acoustic communication channel characterized by wind-generated surface waves and bubbles," *Oceanic Engineering, IEEE Journal of*, vol. 38, no. 4, pp. 642–654, Oct 2013.

[7] P. van Walree, "Propagation and scattering effects in underwater acoustic communication channels," *Oceanic Engineering, IEEE Journal of*, vol. 38, no. 4, pp. 614–631, Oct 2013.

[8] M. Chitre, I. Topor, and T.-B. Koay, "The UNET-2 modem – an extensible tool for underwater networking research," in *Proceedings of IEEE OCEANS'12 Yeosu*, May 2012.

[9] K. Pelekanakis and M. Chitre, "Adaptive sparse channel estimation under symmetric alpha-stable noise," *Wireless Communications, IEEE Transactions on*, vol. 13, no. 6, pp. 3183–3195, 2014.

[10] C. Spearman, "The proof and measurement of association between two things," *The American Journal of Psychology*, vol. 15, no. 1, pp. 72–101, 1904.